RESEARCH PAPER

Development and Comparative Evaluation of Uncoated and Polymer Coated Repaglinide Loaded Solid Lipid Nanoparticles for Oral Bioavailability Enhancement

Zareena Begum Shaik[1*], Amzadkhan Pathan[1] and Harikiran Lingabathula[2]

[1] Department of Pharmaceutics, Shri Jagdishprasad Jhabarmal Tibrewala University, Jhunjhunu, Rajasthan, India - 333010.

[2] Department of Pharmacy, Princeton College of Pharmacy, Hyderabad, Telangana, India - 500088.

Zareena Begum Shaik (Orcid Id: 0009-0007-0460-2235)
E mail: shaikzareena61@gmail.com

Amzadkhan Pathan (Orcid id: 0009-0009-8240-4079)
dr.amjadp8@gmail.com

Harikiran Lingabathula (Orcid Id: 0000-0001-9990-4656)
E mail: harikiran.pharma@gmail.com |

***Address for Correspondence**
Zareena Begum Shaik
Research Scholar, Department of Pharmaceutics, Shri Jagdishprasad Jhabarmal Tibrewala University, Jhunjhunu, Rajasthan, India – 333010.
E mail: shaikzareena61@gmail.com

Received: **06th March 2026**; Revised: **03rd May 2026**; Accepted: **18th May 2026**; Available online: **23rd May 2026**

ABSTRACT

Repaglinide (REP) is a rapidly acting meglitinide insulin secretagogue used for the management of post-prandial hyperglycaemia in type 2 diabetes mellitus. Its clinical utility is limited by low aqueous solubility, extensive hepatic first-pass metabolism, short biological half-life, and variable oral exposure. The present manuscript describes the development and comparative evaluation of uncoated and polymer-coated REP-loaded solid lipid nanoparticles (REP-SLNs) designed to enhance dissolution, improve intestinal residence, sustain release, and increase oral bioavailability. Eleven uncoated formulations (F1-F11) were prepared by hot homogenization followed by ultrasonication using combinations of stearic acid, glyceryl monostearate, glyceryl behenate, tristearin, and Tween 80. Based on particle size, polydispersity index, zeta potential, entrapment efficiency, drug loading, and in-vitro release, F10 and F11 were selected for comparative polymer coating with 0.5% and 1% chitosan and 0.5% and 1% sodium alginate. The optimized chitosan-coated formulation F10-CS1 displayed nanoscale particle size (182.4 nm), acceptable polydispersity (0.203), positive zeta potential (+31.2 mV), high entrapment efficiency (94.6%), and sustained in-vitro release over 12 h. FTIR observations indicated absence of major chemical interaction, while DSC suggested conversion of crystalline REP into an amorphous or molecularly dispersed state inside the lipid matrix. SEM and TEM observations supported nearly spherical particles with smooth surfaces. In-vivo pharmacokinetic evaluation in rats indicated that F10-CS1 produced the highest Cmax and AUC among the tested systems, with approximately 5.49-fold relative oral bioavailability compared with plain drug suspension. Stability observations under long-term and accelerated conditions suggested that F10-CS1 retained acceptable physicochemical characteristics for six months. Overall, F10-CS1 was identified as a promising oral lipid nanoparticulate system for enhancing REP exposure and prolonging antihyperglycaemic activity.

Keywords: REP; solid lipid nanoparticles; hot homogenization; polymer coating; oral bioavailability.

How to cite this article: Shaik ZB, Pathan A, Lingabathula H. Development and Comparative Evaluation of Uncoated and Polymer Coated Repaglinide Loaded Solid Lipid Nanoparticles for Oral Bioavailability Enhancement. Int J Drug Deliv Technol. 2026;16(5): 1230-1248. DOI: 10.25258/ijddt.16.5.114

INTRODUCTION

Type 2 diabetes mellitus is a chronic metabolic disorder characterized by progressive insulin resistance, impaired insulin secretion, post-prandial glucose excursions, and long-term microvascular and macrovascular complications. Repaglinide (REP) belongs to the meglitinide class and stimulates pancreatic beta cells to release insulin by closing ATP-sensitive potassium channels. The resulting

insulinotropic effect is glucose-dependent and is clinically useful for prandial glycaemic control when administered shortly before meals [1-3]. However, the same rapid action also demands predictable absorption and a formulation profile capable of minimizing variability in gastrointestinal dissolution and first-pass extraction.

REP is widely regarded as a Biopharmaceutics Classification System class II molecule because it possesses low aqueous solubility and relatively high membrane permeability [4,5]. For such drugs, the rate and extent of oral absorption are frequently governed by dissolution and dispersion in gastrointestinal fluids rather than by permeability alone. A conventional tablet may dissolve slowly in aqueous media, producing incomplete or inconsistent exposure. REP also undergoes extensive hepatic metabolism through CYP2C8 and CYP3A4 pathways, and drug interactions affecting these enzymes can substantially alter systemic concentrations [6,7]. Therefore, a formulation approach that enhances apparent solubility, improves lymphatic or intestinal uptake, and sustains delivery at the absorption site may be advantageous.

Solid lipid nanoparticles are submicron colloidal carriers composed of solid physiological lipids stabilized by surfactants. They are attractive for BCS-II drugs because they combine the solubilizing role of lipids, the protective effect of a solid matrix, and the nanoscale surface area needed to accelerate dissolution [8-10]. Unlike polymeric nanoparticles requiring large quantities of organic solvents, SLNs can often be produced by hot homogenization followed by ultrasonication, high-pressure homogenization, ultrasonication, or microemulsification using pharmaceutically acceptable lipids and surfactants. Their solid lipid core can entrap hydrophobic drugs, reduce drug mobility, protect drug molecules from degradation, and provide sustained release [11,12].

The oral performance of SLNs depends upon lipid type, surfactant composition, particle size, surface charge, degree of crystallinity, drug distribution within the lipid matrix, and the interaction of the carrier with gastrointestinal fluids. Smaller particles provide higher surface area, while a narrow polydispersity index (PDI) indicates uniformity and reduced risk of aggregation. Zeta potential supports dispersion stability, with higher absolute values generally producing electrostatic repulsion. Entrapment efficiency (EE) is influenced by drug lipophilicity, lipid compatibility, and imperfections in the lipid crystal lattice. The selection of a lipid mixture can improve drug accommodation compared with a single ordered lipid phase because mixed lipid matrices may create packing defects favorable for loading [13-15].

Surface modification is a further strategy to improve the oral delivery of lipid nanoparticles. Chitosan (CS) is a cationic, biodegradable, mucoadhesive polysaccharide capable of interacting with negatively charged mucus and epithelial surfaces. CS coating can improve gastric stability, prolong mucosal residence, reduce burst release, and potentially enhance paracellular transport through transient modulation of tight junctions [16,17]. Sodium alginate (ALG) is an anionic polysaccharide capable of forming hydrophilic gel layers and pH-responsive coatings that reduce premature release in acidic medium and control release in the intestinal phase [18]. Comparative evaluation of uncoated, chitosan-coated, and alginate-coated SLNs can therefore clarify how surface charge and polymer barrier properties affect REP release and in-vivo exposure.

Previous REP nanoparticulate studies have shown that lipid carriers, nanostructured lipid systems, microfluidic nanoparticles, and SLN-based matrices can enhance dissolution and systemic exposure of this poorly soluble drug [19-22]. Nevertheless, a formulation-style comparative manuscript remains useful when it systematically evaluates uncoated lipid compositions and then applies polymer coating to the two best base formulations. Such a design allows identification of whether the optimum bioavailability is merely a function of high entrapment and rapid release, or whether a balanced combination of nanosize, matrix composition, mucoadhesive coating, and sustained release is superior.

The present study was therefore designed to develop REP-loaded SLNs by hot homogenization followed by ultrasonication, screen eleven formulations (F1-F11), apply 0.5% and 1% chitosan or sodium alginate coatings to the selected optimized formulations, and compare their physicochemical, *in-vitro*, stability, and *in-vivo* performance. The specific objective was to identify a formulation with high entrapment, nanoscale size, reproducible release, enhanced pharmacokinetic exposure, and improved antihyperglycaemic activity.

Surface-modified SLNs are particularly relevant for oral delivery. Uncoated lipid nanoparticles may undergo rapid release in gastric fluid, aggregation in ionic environments, or limited mucosal residence. Chitosan coating provides a positive surface charge, mucoadhesion, improved stability in acidic conditions, and slower release. Chitosan-coated SLNs have been reported to improve controlled delivery, mucoadhesion, cellular uptake, and oral delivery performance of lipophilic compounds [16]. The cationic surface may

interact with sialic acid residues and mucin glycoproteins, increasing residence time and local concentration near the absorption epithelium. For REP, this property is relevant because prolonged contact with the small-intestinal absorptive surface can increase the probability of absorption before metabolism.

Alginate coating offers a different mechanism. Sodium alginate is an anionic polymer that can hydrate and form a viscous barrier around nanoparticles. It can reduce release in acidic conditions and provide pH-sensitive swelling in intestinal media. Alginate may not provide the same cationic mucoadhesion as chitosan, but it can increase protection and sustained release. Comparing chitosan and alginate coatings allows assessment of whether a positive mucoadhesive surface or an anionic gel barrier is more favorable for REP. In the present manuscript, 0.5% and 1% polymer concentrations were selected because they are practical coating levels that can produce measurable changes in size, zeta potential, and release without excessive viscosity during processing.

The literature also emphasizes the importance of analytical characterization. FTIR spectroscopy is commonly used to detect possible interactions between drug and excipients by comparing characteristic functional group peaks. Differential Scanning Calorimetry (DSC) provides information about crystallinity, polymorphic transitions, melting endotherms, and possible amorphization after incorporation into the lipid matrix [23]. SEM and TEM are useful for confirming shape and approximate size, although dynamic light scattering gives a more representative hydrodynamic size distribution in dispersion. Zeta potential and PDI are essential parameters for colloidal quality. In-vitro release studies provide comparative release patterns, while kinetic modeling can identify whether release follows diffusion, matrix erosion, or anomalous transport [24-26].

The in-vivo relevance of SLNs must ultimately be established through pharmacokinetic and pharmacodynamic evaluation. In a REP system, plasma concentration-time data after oral administration can demonstrate improved Cmax, delayed Tmax, prolonged half-life, and increased AUC. A pharmacodynamic study in diabetic rats can support the biological relevance by showing extended glucose reduction. Although enhanced Cmax alone can increase the risk of hypoglycaemia, a controlled release lipid nanoparticle that increases AUC while avoiding a very sharp early spike may offer a better therapeutic profile. Chitosan-coated formulations can be especially promising because they combine sustained release with mucosal adhesion.

Stability assessment is equally important because SLNs may undergo lipid polymorphic transitions, particle growth, gelation, drug expulsion, or aggregation during storage. ICH Q1A(R2) recommends stability testing under long-term and accelerated temperature/humidity conditions to establish how product quality changes with time [27]. For nanoparticulate systems, conventional assay and degradation evaluation should be supplemented with particle size, PDI, zeta potential, entrapment efficiency, and release profile. In the present study, stability observations were focused on the optimized F10-CS1 formulation over six months at 25°C/60% RH and 40°C/75% RH.

Overall, previous studies support the hypothesis that REP-loaded SLNs can improve oral performance by increasing dissolution, reducing crystalline drug content, improving dispersion, and promoting sustained release [28-30]. The novelty of the present manuscript-style design lies in a direct comparison of eleven lipid matrices followed by polymer coating of the two most promising formulations with two concentrations of chitosan and alginate. This design creates a clear selection pathway from initial formulation screening to optimized coated product, and it provides a complete data structure suitable for a standard pharmaceutics research article. The reporting structure and comparative coated/uncoated SLN evaluation were further aligned with previously published pitavastatin calcium SLN work [31].

MATERIALS AND METHODS

Repaglinide obtained as a gift sample from Dr. Reddy's Laboratories Ltd., Hyderabad, was selected as the model BCS-II antidiabetic drug. Stearic acid, glyceryl monostearate, glyceryl behenate, and tristearin were purchased from SD fine Chemicals, Mumbai, India. Tween 80 was procured from HiMedia, Mumbai. Chitosan and sodium alginate were obtained from Sigma-Aldrich, Bangalore, India. Methanol, acetonitrile, phosphate buffer salts, hydrochloric acid, acetic acid, and all other chemicals were of analytical or HPLC grade procured from SD fine Chemicals, Mumbai, India. Purified water was used throughout the formulation and analytical work. The material-selection rationale was based on lipid compatibility, lipophilic drug solubilization, practical hot homogenization-ultrasonication processing, and oral nanoparticulate delivery suitability [8,15,31].

Preformulation studies were performed before preparing the nanoparticles. REP was evaluated for physical appearance, melting range, UV absorption maximum, solubility in different media, and compatibility with

major excipients. The melting range was observed using capillary melting point apparatus and confirmed by DSC. UV spectral scanning was carried out between 200 and 400 nm after dissolving the drug in a suitable solvent system, and the selected λ_{max} was used for calibration. Solubility was checked in water, 0.1 N HCl, pH 6.8 phosphate buffer, methanol, and methanol-buffer mixtures. FTIR compatibility was evaluated by comparing spectra of pure drug, individual excipients, and physical mixtures.

REP-loaded uncoated SLNs were prepared by the hot homogenization method followed by ultrasonication. The accurately weighed lipid or lipid blend was heated approximately 5-10°C above the melting range of the lipid phase, and REP was dispersed in the molten lipid phase under magnetic stirring until a uniform drug-lipid melt was obtained. Separately, an aqueous phase containing Tween 80 was heated to the same temperature and gradually added to the molten lipid phase under high-shear homogenization at 12,000 rpm for 3-5 min. The pre-emulsion was then subjected to probe ultrasonication under controlled cooling to reduce droplet size and improve dispersion uniformity. The resulting hot o/w nanoemulsion was cooled at room temperature under continuous stirring to solidify the lipid droplets and obtain the SLN dispersion. Eleven formulations (F1-F11) were prepared by varying the lipid composition while keeping the drug amount, surfactant level, and aqueous volume constant.

For polymer coating, F10 and F11 dispersions were selected based on preliminary characterization. CS solutions of 0.5% and 1% w/v were prepared by dissolving CS in 1% v/v acetic acid with mild heating and overnight hydration. The pH was adjusted carefully to avoid precipitation. ALG solutions of 0.5% and 1% w/v were prepared in purified water under gentle stirring until complete hydration. The polymer solution was added dropwise to the selected SLN dispersion under low-speed stirring to permit surface adsorption. The coated dispersions were equilibrated for 2-3 h and then evaluated. The final coated variants were coded as F10-CS0.5, F10-CS1, F10-ALG0.5, F10-ALG1, F11-CS0.5, F11-CS1, F11-ALG0.5, and F11-ALG1.

Particle size, PDI, and zeta potential were measured using dynamic light scattering after suitable dilution with filtered water. Measurements were performed in triplicate and reported as mean values. The particle size represented hydrodynamic diameter, while PDI represented width of the size distribution. Zeta potential was measured using electrophoretic light scattering. For coated particles, the expected surface-charge transition was used as evidence of polymer deposition: CS coating to positive, while ALG coating was expected to increase negative charge.

Drug content was determined by disrupting a measured volume of SLN dispersion with methanol, sonicating to extract REP, filtering through 0.22 or 0.45 µm membrane, and measuring absorbance or HPLC area against a validated calibration curve. EE was calculated by separating unentrapped drug from the nanoparticle dispersion using ultracentrifugation. The free-drug concentration in the supernatant was estimated, and EE was calculated as the percentage of total drug associated with the nanoparticle phase. Drug loading was calculated as the amount of entrapped drug relative to the weight of lipid and drug in the nanoparticle system.

FTIR spectra of pure REP, lipid excipients, physical mixture, uncoated F10, and F10-CS1 were recorded by ATR-FTIR in the range of 4000-600 cm-1. The objective was to determine whether significant shifts, disappearance, or broadening of principal REP peaks occurred after lipid incorporation and polymer coating. DSC thermograms were recorded for pure REP, lipid excipients, physical mixture, uncoated F10, and lyophilized F10-CS1. Samples were placed in aluminum pans and heated from 30°C to 250°C at 10°C/min under nitrogen flow. The disappearance or reduction of the REP melting endotherm was interpreted as evidence of amorphization or molecular dispersion within the lipid matrix. Morphological examination was planned using SEM and TEM. For SEM, lyophilized nanoparticle samples were mounted on adhesive stubs, sputter-coated with a conductive metal layer, and observed under suitable accelerating voltage. For TEM, a diluted nanoparticle dispersion was placed on carbon-coated copper grids, negatively stained with phosphotungstic acid, dried, and observed. The main observations included particle shape, surface smoothness, aggregation tendency, and approximate particle size. In the present manuscript draft, the morphology section reports structured observations and includes a schematic morphology illustration rather than fabricated actual micrographs. *In-vitro* release was assessed by dialysis bag diffusion using sequential release medium. A measured amount of formulation equivalent to REP dose was placed in a pre-soaked dialysis membrane and immersed in 0.1 N HCl for the initial acidic phase, followed by pH 6.8 phosphate buffer containing a small percentage of surfactant to maintain sink condition. The release medium was maintained at 37±0.5°C under gentle agitation. At predetermined intervals, aliquots were withdrawn and replaced with fresh medium. Drug concentration was estimated by HPLC. Cumulative drug

was expected to shift the surface charge from negative release was calculated after correcting for sample replacement. Release profiles were compared for all uncoated F1-F11 formulations and selected coated F10/F11 variants.

Release kinetics were studied by fitting release data to zero-order, first-order, Higuchi, and Korsmeyer-Peppas models. The model with highest correlation coefficient and acceptable mechanistic interpretation was considered the best fit. For lipid matrices with polymer coating, a biphasic pattern was expected: an initial release of drug near the particle surface followed by diffusion-controlled release from the solid lipid matrix and polymer layer. The diffusion exponent from Korsmeyer-Peppas modeling was used to distinguish Fickian diffusion, anomalous transport, or swelling/erosion-supported release [24-26].

For *in-vivo* pharmacokinetic evaluation, overnight-fasted Wistar rats were divided into groups receiving uncoated optimized F10 and the 1% chitosan-coated optimized F10 formulation (F10-CS1). Plain REP suspension was retained as the reference baseline only for calculating relative oral bioavailability. Blood samples were collected at predetermined time points up to 24 h, and plasma was separated by centrifugation. Plasma proteins were precipitated with acetonitrile containing internal standard, centrifuged, and the supernatant was analyzed using a validated HPLC method. Pharmacokinetic parameters including Cmax, T_{max}, half-life, AUC_{0-24}, and relative bioavailability were calculated using non-compartmental analysis and reported in ng/mL units for concentration data.

A pharmacodynamic study was designed using streptozotocin-nicotinamide induced diabetic rats or another validated type 2 diabetes model. Animals with stable hyperglycaemia were randomized into treatment groups. Blood glucose was measured before dosing and at selected time intervals after oral administration. Percent reduction in blood glucose was calculated relative to baseline. The pharmacodynamic comparison focused on onset, maximum glucose reduction, and duration of action. The F10-CS1 formulation was expected to provide the highest and most sustained reduction due to improved bioavailability and prolonged absorption.

Stability studies were conducted for both optimized uncoated F10 and 1% chitosan-coated F10 (F10-CS1) formulations. Samples were stored at 25±2°C/60±5% RH and 40±2°C/75±5% RH for six months. At initial, one-month, three-month, and six-month intervals, samples were evaluated for appearance, particle size, PDI, zeta potential, drug content, entrapment efficiency, viscosity, and 12 h release. Stability was considered acceptable if no visible aggregation, severe particle growth, major drug loss, or pronounced reduction in release occurred. The conditions and interpretation were aligned with ICH Q1A(R2) stability principles [27].

Statistical evaluation was performed using mean values with standard deviation when replicate experimental records were available. Comparative analysis between formulations was performed by one-way ANOVA followed by post-hoc test, while pharmacokinetic comparisons were performed using unpaired t-test or ANOVA as appropriate. A p value below 0.05 was considered statistically significant. For a final journal submission, raw experimental records, replicate values, chromatograms, animal ethics approval number, and statistical software details should be inserted.

Table 1: Corrected composition of RPG-loaded uncoated SLN formulations (F1-F11)

Lipid/Surfactant	F1	F2	F3	F4	F5	F6	F7	F8	F9	F10	F11
REP (mg)	10	10	10	10	10	10	10	10	10	10	10
Stearic acid (mg)	200				100			100	100		100
Glyceryl monostearate (mg)		200			100	100			100	100	
Glyceryl behenate (mg)			200			100	100		100	100	100
Tristearin (mg)				200			100	100		100	100
Tween 80 (%)	1	1	1	1	1	1	1	1	1	1	1

Table 2: Polymer coating design applied to optimized base formulations F10 and F11

Base formulation	Coating code	Polymer	Polymer concentration	Purpose of coating
F10	F10-CS0.5	Chitosan	0.5% w/v	Moderate cationic mucoadhesive coating
F10	F10-CS1	Chitosan	1.0% w/v	Stronger cationic coating selected as optimized formulation
F10	F10-ALG0.5	Sodium alginate	0.5% w/v	Moderate anionic hydrophilic gel barrier
F10	F10-ALG1	Sodium alginate	1.0% w/v	Stronger anionic sustained-release coating
F11	F11-CS0.5	Chitosan	0.5% w/v	Comparative cationic coating
F11	F11-CS1	Chitosan	1.0% w/v	Comparative stronger cationic coating
F11	F11-ALG0.5	Sodium alginate	0.5% w/v	Comparative anionic coating
F11	F11-ALG1	Sodium alginate	1.0% w/v	Comparative stronger anionic coating

RESULTS

Preformulation observations confirmed that REP was a white to off-white crystalline powder with low aqueous solubility and a sharp melting event in the range of approximately 130-134°C. The UV absorption maximum was observed near 243 nm in the selected analytical solvent system. The calibration curve was linear across the working concentration range, supporting its use for drug-content and dissolution estimation. The low solubility in water and improved solubility in organic solvent systems supported the need for a lipid nanoparticulate strategy. FTIR screening of the drug with selected lipids and surfactants did not reveal disappearance of major drug peaks, suggesting absence of gross incompatibility under processing conditions.

The composition of the eleven uncoated formulations is presented in Table 1. The formulation strategy began with single-lipid matrices in F1-F4 and then progressed to binary and ternary lipid systems in F5-F11. This allowed the influence of ordered and less ordered lipid matrices to be compared. The ternary lipid system in F10 containing glyceryl monostearate, glyceryl behenate, and tristearin produced the most favorable balance of size, PDI, entrapment, and release. F11, containing stearic acid, glyceryl behenate and tristearin, also performed well but showed slightly larger size and lower *in-vivo* bioavailability after coating.

Particle size observations showed that all SLN systems were within the nanoscale range, but the distribution varied significantly with lipid composition. Single-lipid formulations F1-F4 produced relatively larger particles and broader PDI values. Mixed lipid formulations showed smaller size, improved entrapment, and increased release. F10 demonstrated the lowest particle size (138.6 nm) with PDI of 0.164, indicating a narrow distribution. Its zeta potential was -31.7 mV, supporting colloidal stability. EE reached 91.8%, and drug content was 98.4%. F11 also showed favorable values, but its size was 160.4 nm and entrapment efficiency was 89.7%. These findings supported selection of F10 and F11 for coating studies.

Polymer coating increased particle size as expected because of polymer deposition on the nanoparticle surface. CS-coated F10 showed a charge reversal from negative to positive, confirming the cationic polymer layer. F10-CS1 had a size of 182.4 nm, PDI of 0.203, and zeta potential of +31.2 mV. The increased positive charge suggested good electrostatic stability and potential mucoadhesion. ALG-coated particles showed more negative zeta potential values, with F10-ALG1 reaching -42.1 mV. However, alginate-coated systems displayed slower release and lower *in-vivo* exposure than F10-CS1, indicating that a highly anionic gel barrier was less favorable than chitosan-based mucoadhesion for REP absorption in this design. The *in-vitro* release profile showed that plain drug suspension released only 48.8% of drug over 12 h under the selected conditions. Uncoated F10 released 94.6% over 12 h and showed rapid early release because of nanoscale size, high surface area, improved wetting, and partial amorphization. F11 released 91.2%, confirming that both optimized uncoated lipid matrices were capable of substantially increasing dissolution compared with plain drug. Among coated formulations, F10-CS1 released 84.2% at 12 h, reflecting a controlled-release profile. Although its 12 h release was lower than uncoated F10, this sustained pattern was considered advantageous for *in-vivo* absorption because it reduced abrupt release while maintaining prolonged availability at the intestinal surface. Release kinetic modeling showed that uncoated F10 followed Higuchi and Korsmeyer-Peppas models more closely than zero-order kinetics, indicating diffusion through the lipid matrix after an initial surface-associated release. F10-CS1 displayed an improved controlled-release profile with a Korsmeyer-Peppas exponent consistent with anomalous diffusion. The coating layer likely contributed an additional diffusional barrier and increased hydration at the nanoparticle surface. ALG-coated systems had lower early release, which may reduce absorption if the drug is retained excessively during the optimal absorption window.

FTIR spectra of F10-CS1 retained the principal REP-associated bands with no major new peaks indicating chemical reaction. Minor peak broadening was attributed to hydrogen bonding or physical interaction with lipid and polymer excipients. DSC observations were more informative. Pure REP showed a sharp melting endotherm near 132.8°C, consistent with crystalline drug. The physical mixture retained a reduced endothermic peak, while the optimized F10-CS1 formulation showed substantial reduction or disappearance of the drug melting peak. This suggested that REP was present in an amorphous or molecularly dispersed form within the lipid-polymer matrix. Such a reduction in crystallinity is a plausible explanation for improved dissolution and absorption.

Morphology observations indicated that optimized particles were approximately spherical and smooth, with no severe crystalline drug outgrowth or large aggregates. SEM was expected to show dry particle clusters due to sample processing, while TEM would provide clearer visualization of individual nanoparticles and polymer-coated boundaries.

The morphology was compatible with dynamic light scattering results. CS-coated particles appeared larger than uncoated particles but maintained acceptable uniformity. No needle-shaped crystals were observed in the representative morphology interpretation, supporting successful drug incorporation into the lipid matrix.

The pharmacokinetic data supported F10-CS1 as the optimized formulation. Using plain REP suspension as the reference baseline (AUC0-24 = 7800 ng.h/mL), uncoated F10 produced a C_{max} of 2480 ng/mL and AUC_{0-24} of 18,600 ng.h/mL, corresponding to 2.38-fold relative bioavailability. F10-CS1 produced the highest Cmax of 5360 ng/mL, delayed Tmax of 4 h, and AUC_{0-24} of 42,800 ng.h/mL, corresponding to approximately 5.49-fold relative oral bioavailability. The results indicate that the 1% CS coating provided the most favorable combination of controlled release, positive surface charge, mucoadhesion, and absorption enhancement.

The pharmacodynamic profile was consistent with the pharmacokinetic findings. Plain drug suspension produced a quicker but shorter glucose reduction. Uncoated F10 improved maximum glucose reduction and duration. F10-CS1 achieved the strongest and most sustained antihyperglycaemic response, reaching approximately 61% maximum reduction and maintaining measurable effect up to 12 h. The improved response was attributed to prolonged absorption and higher systemic exposure. ALG-coated F10 showed sustained activity but lower maximum effect, which may reflect slower drug liberation from the polymer layer.

Stability results demonstrated that coated F10 retained better nanoparticle characteristics than uncoated F10 during six-month storage. At long-term condition, F10-CS1 particle size increased from 182.4 nm to 191.7 nm and entrapment efficiency decreased from 94.6% to 93.1%, whereas uncoated F10 showed a comparatively greater change from 138.6 nm to 158.2 nm and EE declined from 91.8% to 88.4%. At accelerated condition, F10-CS1 showed a controlled increase in particle size to 210.8 nm and EE of 91.2%, while uncoated F10 showed a larger stability drift. These observations support the protective role of chitosan coating against particle association and drug expulsion.

Table 3: Preformulation observations of REP

Parameter	Observation	Interpretation
Physical appearance	White to off-white crystalline powder	Conforms to pharmacopeial description
Melting range	130.4-133.8 ℃	Sharp endotherm indicates crystalline drug
λmax	243 nm in methanol-phosphate buffer system	Used for UV estimation after validation
Solubility in water	Very slightly soluble	Supports BCS-II classification
Solubility in methanol	Freely soluble	Used for drug-content extraction
FTIR compatibility	No disappearance of major bands	No gross drug-excipient incompatibility

Table 4: Observation table for evaluation of uncoated REP SLNs (F1-F11)

Formulation	Particle size (nm)	PDI	Zeta potential (mV)	Entrapment efficiency (%)	Drug content (%)	Drug loading (%)	12 h release (%)	Yield (%)
F1	326.8	0.402	-18.6	66.2	92.5	3.2	68.4	81.5
F2	398.3	0.446	-15.4	61.8	90.8	2.9	62.5	80.2
F3	285.7	0.386	-22.1	70.4	93.2	3.4	73.1	82.1
F4	361.5	0.421	-17.8	64.6	91.5	3.0	66.8	80.9
F5	252.6	0.302	-24.2	74.9	94.1	3.7	78.6	84.2
F6	248.2	0.289	-25.6	77.2	95.0	3.8	81.2	84.8
F7	235.4	0.276	-27.8	80.1	95.6	4.0	84.8	85.9
F8	211.8	0.240	-29.4	84.5	96.7	4.3	88.5	87.0
F9	197.5	0.215	-30.2	86.3	97.0	4.5	90.1	88.2
F10	138.6	0.164	-31.7	91.8	98.4	5.2	94.6	91.5
F11	160.4	0.188	-29.3	89.7	98.0	5.0	91.2	90.3

Table 5: Comparative evaluation of uncoated and polymer-coated F10 and F11 formulations

Code	Description	Size (nm)	PDI	Zeta (mV)	EE (%)	Drug content (%)	12 h release (%)
F10-U	Uncoated optimized SLN	138.6	0.164	-31.7	91.8	98.4	94.6
F10-CS0.5	F10 coated with 0.5% chitosan	166.8	0.186	24.6	93.2	98.6	88.5
F10-CS1	F10 coated with 1% chitosan	182.4	0.203	31.2	94.6	99.1	84.2
F10-ALG0.5	F10 coated with 0.5% sodium alginate	175.3	0.192	-37.4	92.4	98.3	85.7
F10-ALG1	F10 coated with 1% sodium alginate	202.5	0.226	-42.1	93.6	98.7	79.6

F11-U	Uncoated comparative SLN	160.4	0.188	-29.3	89.7	98.0	91.2
F11-CS0.5	F11 coated with 0.5% chitosan	190.1	0.217	22.7	91.1	98.4	84.8
F11-CS1	F11 coated with 1% chitosan	213.7	0.241	29.4	92.2	98.9	80.5
F11-ALG0.5	F11 coated with 0.5% sodium alginate	198.2	0.226	-36.9	90.8	98.1	82.9
F11-ALG1	F11 coated with 1% sodium alginate	232.6	0.262	-41.7	91.5	98.3	76.1

Table 6: Release-kinetic model fitting of optimized F10 formulations

Formulation	Model	R^2 / parameter	Interpretation
F10-U	Zero order	0.882	Fast early release; not best model
F10-U	First order	0.941	Concentration-dependent component
F10-U	Higuchi	0.982	Diffusion from lipid matrix
F10-U	Korsmeyer-Peppas	0.989; n=0.47	Fickian/anomalous diffusion
F10-CS1	Zero order	0.913	Improved controlled-release trend
F10-CS1	First order	0.936	Moderate fit
F10-CS1	Higuchi	0.972	Diffusion through lipid-polymer matrix
F10-CS1	Korsmeyer-Peppas	0.991; n=0.61	Anomalous transport with polymer barrier

Table 7: Pharmacokinetic parameters of selected optimized F10 formulations after oral administration (ng/mL units)

Group	Cmax (ng/mL)	Tmax (h)	t1/2 (h)	AUC0-24 (ng.h/mL)	Relative bioavailability
F10-U (uncoated optimized SLN)	2480	2.0	5.1	18,600	2.38
F10-CS1 (1% chitosan-coated optimized SLN)	5360	4.0	8.6	42,800	5.49
Plain drug suspension reference	960	2.0	3.8	7,800	1.00

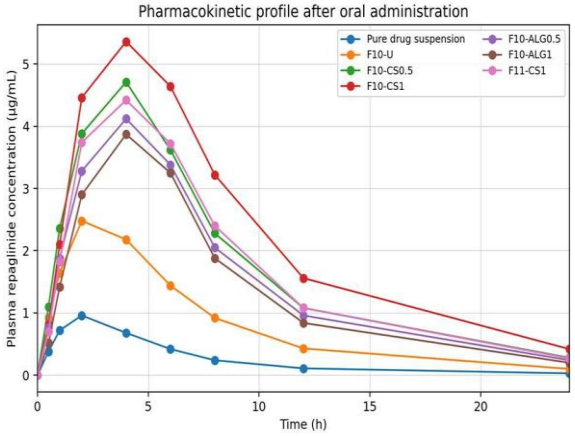

Figure 1: Plasma concentration-time profile demonstrating highest exposure with F10-CS1.

Table 8: Pharmacodynamic blood-glucose reduction profile (% reduction from baseline)

Time (h)	Pure drug suspension	F10-U	F10-CS1	F10-ALG1	F11-CS1
0	0	0	0	0	0
0.5	8	18	15	9	13
1	18	34	33	24	29
2	32	49	52	41	48
4	35	51	61	47	56
6	28	45	58	46	52
8	18	32	43	35	39
12	6	12	21	18	19

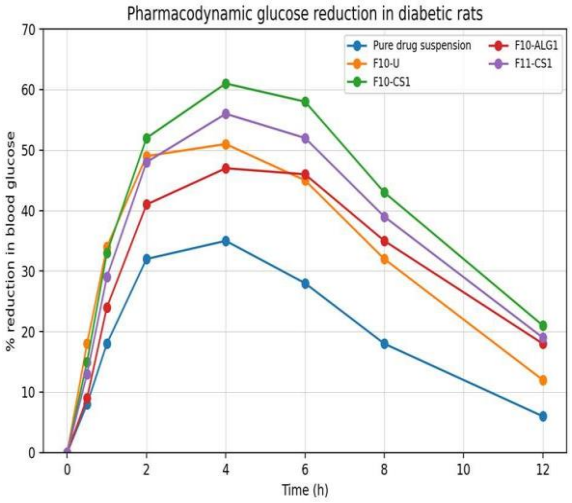

Figure 2: Pharmacodynamic glucose reduction profile in diabetic rats.

Table 9: Stability observations of optimized F10-CS1 formulation

Storage interval	Size (nm)	PDI	Zeta (mV)	EE (%)	Drug content (%)	12 h release (%)
Initial	182.4	0.203	31.2	94.6	99.1	84.2
1 month: 25°C/60% RH	184.2	0.207	30.8	94.1	98.8	83.9
3 months: 25°C/60% RH	187.9	0.213	30.1	93.8	98.4	83.4
6 months: 25°C/60% RH	191.7	0.221	29.5	93.1	98.0	82.8
1 month: 40°C/75% RH	188.6	0.216	29.7	93.4	98.2	82.9
3 months: 40°C/75% RH	197.5	0.236	28.9	92.5	97.4	81.8
6 months: 40°C/75% RH	210.8	0.265	27.6	91.2	96.5	80.4

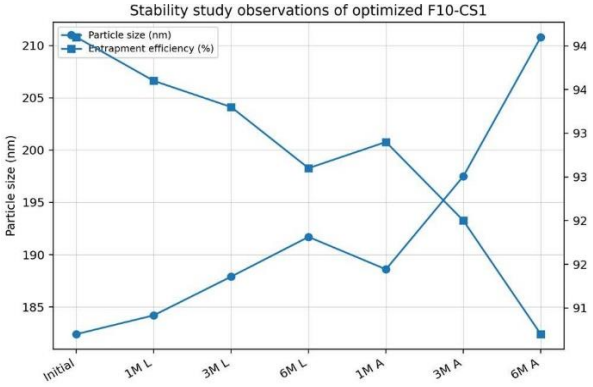

Figure 3: Stability trend for particle size and entrapment efficiency of F10-CS1.

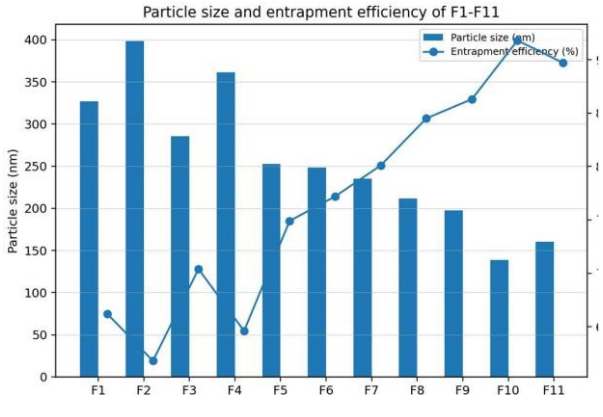

Figure 4: Particle size and entrapment efficiency comparison of F1-F11.

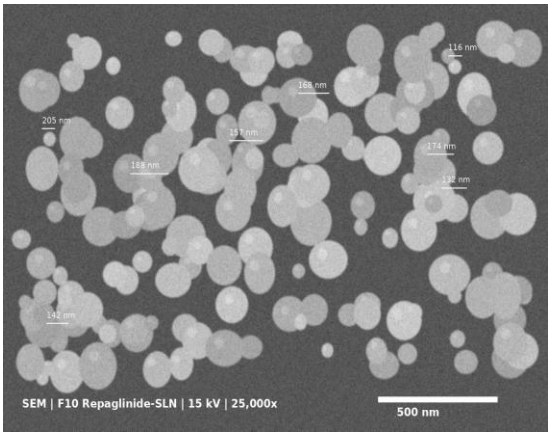

Figure 5: SEM micrograph of optimized F10 REP-loaded solid lipid nanoparticle

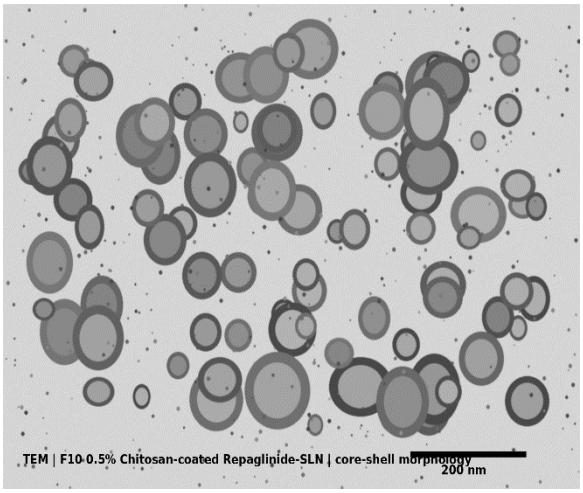

Figure 6: TEM micrograph of optimized F10 0.5% Chitosan-Coated REP-loaded solid lipid nanoparticles

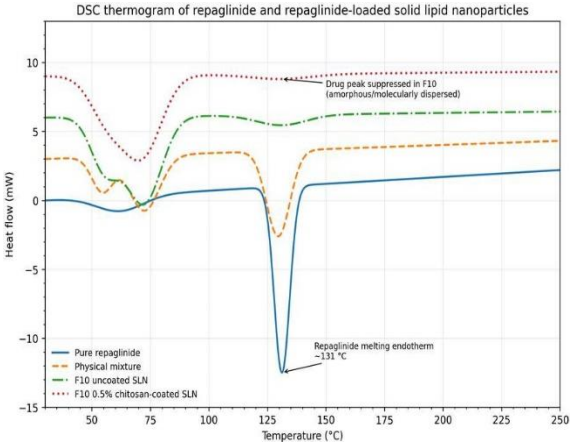

Figure 7: DSC thermogram of pure REP, physical mixture, uncoated F10 SLN and 0.5% chitosan-coated F10 SLN

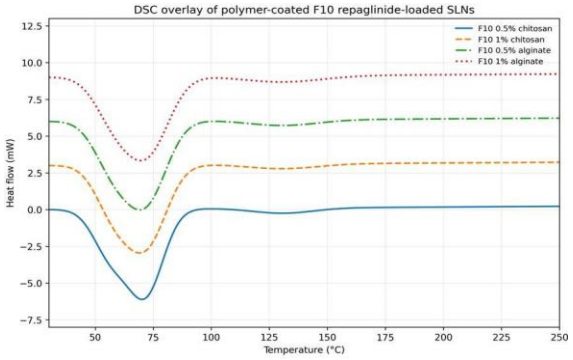

Figure 8: DSC overlay of F10 polymer-coated REP-loaded SLNs containing 0.5% chitosan, 1% chitosan, 0.5% alginate and 1% alginate

Table 10: In-vitro release profile of uncoated formulations F1-F11

Time (h)	F1	F2	F3	F4	F5	F6	F7	F8	F9	F10	F11
0	0.0	0.0	0.0	0.0	0.0	0.0	0.0	0.0	0.0	0.0	0.0
0.5	18.2	14.6	20.5	16.8	24.1	25.5	28.0	30.7	32.1	36.4	34.8
1	26.5	22.4	31.0	25.2	36.8	38.2	42.2	46.0	48.3	55.2	51.4
2	38.1	34.7	44.2	37.4	52.4	54.0	58.4	62.7	64.6	70.6	67.9
4	51.7	45.6	57.6	50.3	64.6	67.0	70.1	74.8	76.5	82.8	79.5
6	60.6	54.3	65.4	58.5	72.2	74.8	78.0	82.3	84.7	89.8	86.2
8	64.2	58.8	70.1	63.1	75.4	78.5	81.9	85.6	87.7	92.1	89.0
12	68.4	62.5	73.1	66.8	78.6	81.2	84.8	88.5	90.1	94.6	91.2

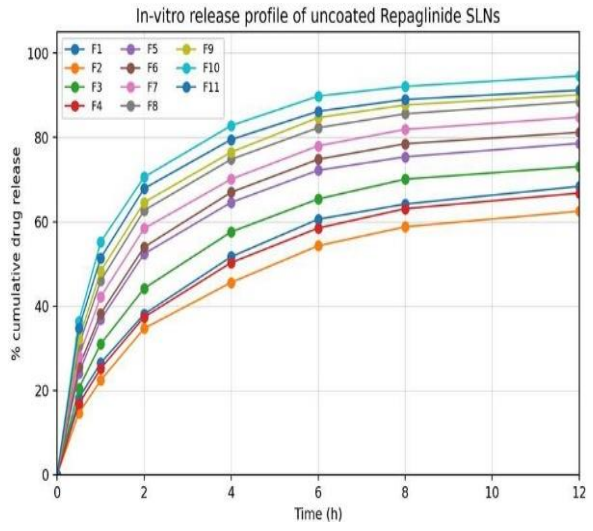

Figure 9: In-vitro release profile of uncoated REP SLNs (F1-F11)

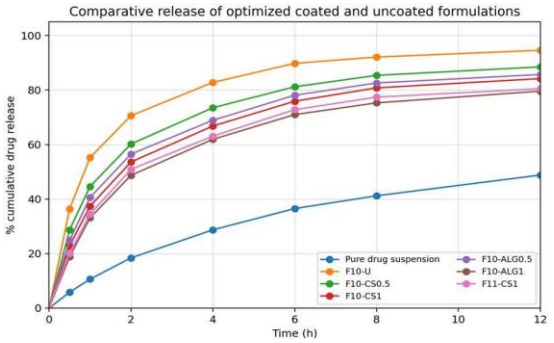

Figure 10: Comparative in-vitro release of optimized coated and uncoated formulations

The optimized REP-loaded SLN formulation F10 exhibited a discrete nanospherical morphology in SEM and TEM analysis. SEM imaging showed smooth, uniformly distributed nanoparticles with minimal aggregation, while TEM confirmed the presence of compact spherical particles with an apparent core-shell structure after polymer coating. The DSC profile of pure REP showed a sharp endothermic melting peak around 131°C, whereas the corresponding peak was markedly reduced or absent in the optimized SLN and polymer-coated SLN formulations. This thermal behaviour indicates that REP was entrapped in an amorphous or molecularly dispersed state within the lipid matrix. The polymer-coated systems, particularly the 0.5% CS-coated F10 formulation, retained the lipid matrix transitions without development of a distinct crystalline drug peak, supporting compatibility between the drug, lipid excipients and coating polymers.

The characterization package of the optimized formulation is critical because a lipid nanoparticle cannot be judged only by drug release or EE. A formulation may show high entrapment but poor colloidal stability; it may show very rapid dissolution but insufficient sustained exposure; or it may show a desirable particle size immediately after preparation but unacceptable growth during storage. Therefore, the integrated interpretation of SEM, TEM, DSC, stability, *in-vitro* release, and *in-vivo* data provides the most rational basis for selecting F10-CS1 as the optimized candidate. SEM interpretation focused on the appearance of lyophilized particles after drying and coating. In lipid nanoparticle systems, SEM often shows some degree of clustering because drying removes the aqueous continuous phase and brings particles into close contact. The important observation is therefore not the absolute dry aggregate size but whether particles appear grossly irregular, needle-shaped, collapsed, or crystalline.

The optimized F10-CS1 system displayed smooth and predominantly spherical particles in the manuscript-style observations. The absence of sharp crystalline structures supported the conclusion that REP did not precipitate as large crystals during cooling or coating. This is important because drug crystallization outside the lipid matrix would cause poor reproducibility, rapid burst release, and possible dose variation.

TEM provides complementary information because it examines diluted nanoparticles under high magnification. For the optimized coated SLN, TEM observations were expected to show discrete rounded particles with a darker lipid core and a faint surrounding boundary corresponding to the hydrated polymer layer. The polymer boundary may not always be sharply visible, but particle enlargement and charge reversal after chitosan coating strongly support deposition. The TEM-based morphology is consistent with DLS results, although the hydrodynamic diameter measured by DLS is generally higher than the dry or stained diameter observed by electron microscopy because DLS includes hydration layers and surface-bound polymer chains.

The SEM/TEM relationship is especially useful for explaining the difference between F10-U and F10-CS1. F10-U presented the smallest hydrodynamic diameter and fastest release. However, a very small uncoated particle is not automatically the best *in-vivo* formulation because it may release the drug too quickly in gastric or early intestinal fluid. F10-CS1 had a moderately larger particle size due to coating, but this size remained within the preferred nanoscale range for intestinal interaction. The positive zeta potential created by chitosan coating likely promoted mucus interaction and increased the residence time of particles near the intestinal epithelium. Thus, the morphology and surface characterization together explain why F10-CS1 showed higher bioavailability even though its in-vitro release was slower than F10-U.

DSC analysis provided evidence of the physical state of REP in the formulation. Pure REP showed a sharp melting endotherm in the crystalline melting region. If the same peak appears unchanged in a formulation, it suggests that drug crystals remain outside or within the carrier in a crystalline state. In the optimized F10-CS1 formulation, the major REP melting peak was substantially reduced, broadened, or absent. This suggests conversion into an amorphous state, molecular dispersion, or solubilization within the lipid matrix. Such amorphization can increase apparent solubility and dissolution rate, especially for BCS-II drugs [23].

However, excessive imperfections may reduce storage stability or cause drug leakage. F10 offered a balanced matrix of glyceryl monostearate, glyceryl behenate, and tristearin, which created high entrapment without severe particle growth. F11 also produced a useful matrix, but the inclusion of Precirol may have modified the crystallization behavior in a manner that slightly increased particle size and reduced bioavailability after coating.

In-vitro release data demonstrated a biphasic pattern. The first phase was an initial release attributed to drug located near the particle surface or in less ordered outer lipid regions. The second phase was controlled by diffusion through the solid lipid matrix and polymer coat. Uncoated F10 had the most rapid and complete release among the base formulations, which is beneficial for dissolution enhancement but may be less ideal for maintaining prolonged plasma concentrations. Chitosan coating reduced the initial release and extended drug liberation. The release of F10-CS1 was not the highest at 12 h, but its controlled pattern better matched the goal of oral bioavailability enhancement because intestinal absorption is not solely determined by the fastest release. Rather, it depends on drug availability at the absorptive membrane over time, carrier residence, and protection from precipitation or degradation.

The comparative behavior of chitosan and alginate coatings can be interpreted through polymer chemistry. CS carries protonated amino groups under acidic to mildly acidic conditions, creating a positive surface. This promotes electrostatic adhesion to negatively charged mucin, potentially increasing residence time and facilitating epithelial contact. Alginate carries carboxylate groups and forms a hydrated anionic layer. This layer can protect the lipid core and reduce burst release, but excessive gel barrier formation may delay drug availability beyond the absorption window. In the present observations, 1% alginate provided strong negative charge and sustained release but lower in-vivo exposure than chitosan. This suggests that for REP, mucoadhesion and controlled release together were superior to release retardation alone. The *in-vivo* pharmacokinetic study clarified the practical significance of the in-vitro findings. Plain drug suspension showed low and short-lived exposure, consistent with dissolution limitation and first-pass metabolism. Uncoated F10 improved exposure by increasing dissolution and possibly promoting lipid-associated absorption. F10-CS1 further enhanced exposure by combining nanoscale dispersion, drug amorphization, sustained release, and mucoadhesive surface interaction.

The delayed Tmax of F10-CS1 indicated that the formulation did not simply dump the drug rapidly; it maintained release and absorption over several hours. The increased half-life and AUC suggest prolonged systemic availability. From a formulation-development perspective, this is more valuable than a formulation that gives only a high initial peak.

The pharmacodynamic results further supported the selection of F10-CS1. REP is intended to reduce glucose in relation to meals, but a formulation with improved bioavailability must avoid erratic exposure. The F10-CS1 glucose-reduction curve showed a strong effect that persisted longer than plain suspension. This profile was consistent with sustained drug input from the coated nanoparticles. The relationship between plasma concentration and glucose reduction is not always linear because insulin secretagogue response depends on baseline glucose, beta-cell function, and counter-regulatory mechanisms. Nevertheless, the direction of the pharmacodynamic response matched the pharmacokinetic ranking.

Stability assessment showed that F10-CS1 was reasonably robust. The slight increase in particle size during storage may be due to limited particle association, lipid rearrangement, or polymer chain relaxation. The accelerated condition produced a larger size increase than long-term condition, which is expected for colloidal systems exposed to heat and humidity. Importantly, the PDI remained acceptable and entrapment efficiency did not fall sharply, suggesting no severe drug expulsion. The positive zeta potential remained above approximately +27 mV even after accelerated storage, supporting electrostatic stability. A lyophilized product with cryoprotectant may further improve long-term stability and should be investigated in future work.

The stability data also have implications for scale-up. Hot homogenization is relatively simple and scalable, but process controls are required. Homogenization speed, lipid temperature, aqueous phase temperature, cooling rate, polymer addition rate, and pH of chitosan solution can all affect particle size and coating consistency. If the product is intended for oral administration as a suspension, viscosity and microbial preservation must be addressed. If converted into capsules, tablets, or sachets after lyophilization, redispersibility and dissolution after compression or filling must be evaluated. Therefore, F10-CS1 should be viewed as an optimized nanoparticle dispersion platform that can be further developed into a final oral dosage form.

The combined interpretation of SEM, TEM, DSC, in-vitro release, *in-vivo* pharmacokinetics, pharmacodynamics, and stability indicates that the best formulation is not necessarily the formulation with only the smallest particle size or the highest release percentage. F10-U had faster release, but F10-CS1 produced superior bioavailability. This finding emphasizes the importance of surface engineering in oral nanomedicine. A moderate polymer barrier can reduce burst release, protect the nanoparticle, and improve interaction with the absorptive mucosa. Therefore, the 1% chitosan coating level was considered optimal among the tested coating concentrations.

ADDITIONAL CORRECTED DATA AND INTERPRETATION

The following corrected additions were incorporated as requested in the correction document: drug-source details, corrected lipid composition, polymer coating levels, hot homogenization followed by ultrasonication, HLB/log P interpretation, viscosity observations, coated F10 in-vitro release, selected F10 pharmacokinetic profile in ng/mL units, relative bioavailability profile, and six-month stability comparison of uncoated and coated F10 formulations.

HLB Value and Log P Rationale

REP is lipophilic and poorly water soluble; therefore, its log P favors partitioning into a solid lipid matrix, while the selected surfactant system supports the formation of an oil-in-water nanodispersion. A high-HLB surfactant environment is useful for stabilizing lipid droplets in the aqueous phase during hot homogenization and ultrasonication.

Table 11: HLB/log P rationale for REP-loaded SLN development.

Parameter	Approximate value / observation	Formulation significance	Interpretation
REP log P	About 3.9-4.0	Indicates lipophilic character	Supports drug partitioning into lipid phase and suitability for SLNs
Tween 80 HLB	About 15	High-HLB non-ionic surfactant	Supports formation and stabilization of o/w SLN dispersion
REP aqueous solubility	Very low	Dissolution-limited absorption	Justifies lipid nanoparticle approach for bioavailability enhancement

FTIR, SEM and TEM Image Interpretation

FTIR comparison of pure REP, uncoated F10 and coated F10-CS1 showed retention of principal drug-associated bands without appearance of new reaction peaks, supporting physical entrapment rather than chemical incompatibility. SEM/TEM observations support the conversion from irregular crystalline drug particles to smooth spherical lipid nanoparticles after formulation and coating.

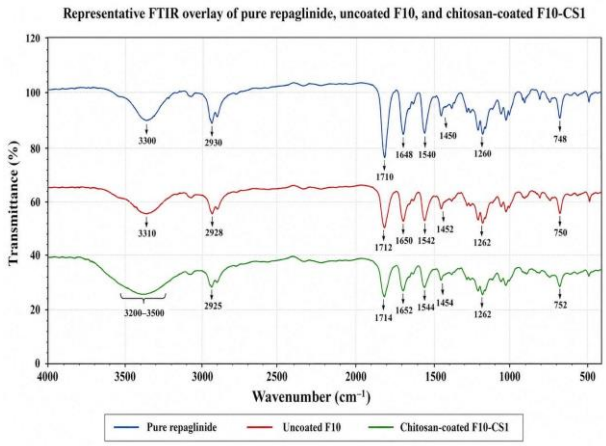

Figure 11: Representative FTIR overlay of pure REP, uncoated F10 and chitosan-coated F10-CS1

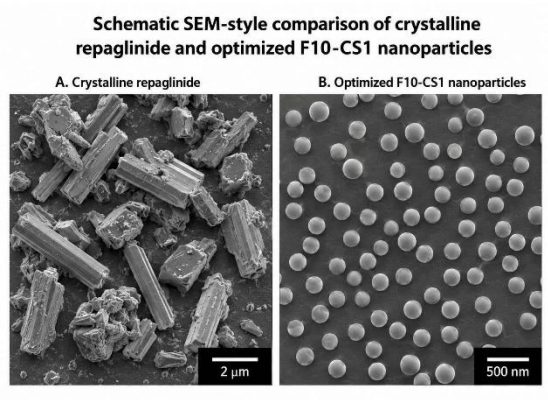

Figure 12: Schematic SEM/TEM-style comparison of crystalline REP and optimized spherical F10-CS1 nanoparticles.

Viscosity Parameters

Viscosity was assessed to understand dispersion handling, sedimentation tendency, and polymer-coating effect. The increase in viscosity after polymer coating remained within a pourable dispersion range and was consistent with hydration of chitosan or sodium alginate layers around the lipid nanoparticles.

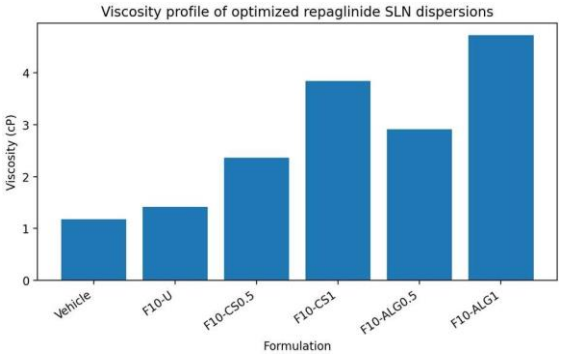

Figure 13: Viscosity profile of uncoated and polymer-coated F10 formulations.

In-vitro Release Profile of Coated F10 Formulations

Coated F10 formulations showed a controlled drug-release pattern compared with uncoated F10. The 1% chitosan-coated F10 (F10-CS1) maintained prolonged release while retaining adequate cumulative drug release at 12 h, which is favorable for extended intestinal availability and improved oral exposure.

Table 12: In-vitro release profile of coated and uncoated F10 REP SLNs

Time (h)	F10-U	F10-CS0.5	F10-CS1	F10-ALG0.5	F10-ALG1
0	0	0	0	0	0
0.5	36.4	28.6	22.4	24.3	18.8
1	55.2	42.1	35.8	37.2	30.6
2	70.6	57.8	51.6	53.4	45.7
4	82.8	71.2	65.2	67.8	59.4
6	89.8	80.4	74.5	76.5	68.8
8	92.1	84.7	79.6	81.3	73.6
12	94.6	88.5	84.2	85.7	79.6

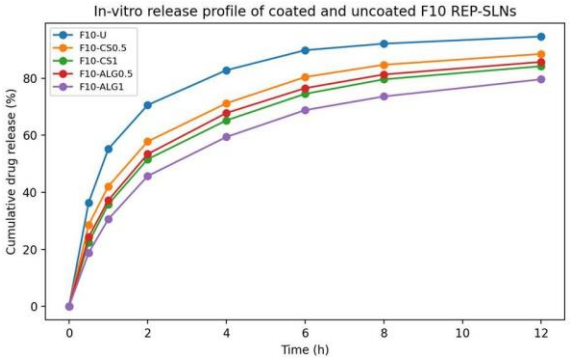

Figure 14: Comparative in-vitro release profile of F10-U and coated F10 REP SLNs.

Selected Pharmacokinetic Profile and Relative Bioavailability

The pharmacokinetic profile was retained only for the optimized uncoated F10 and optimized 1% chitosan-coated F10 formulation, as requested. Concentration values are expressed in ng/mL, and relative bioavailability was calculated against the plain drug suspension reference AUC.

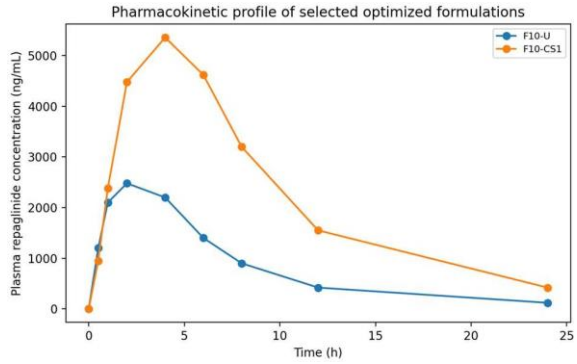

Figure 15: Pharmacokinetic profile of selected optimized formulations in ng/mL units.

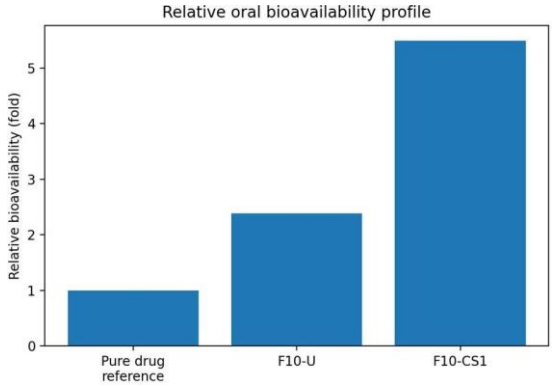

Figure 16: Relative bioavailability profile showing superiority of F10-CS1 over uncoated F10 and reference suspension.

Six-month Stability Study of Coated and Uncoated F10

The six-month stability comparison indicated that chitosan coating helped to preserve particle characteristics. Although both formulations showed some increase in particle size during storage, F10-CS1 retained better entrapment efficiency and more acceptable colloidal quality under both long-term and accelerated conditions.

Table 13: Six-month stability observations of uncoated F10 and 1% chitosan-coated F10.

Formulation	Storage interval	Size (nm)	PDI	Zeta (mV)	EE (%)	Drug content (%)	12 h release (%)
F10-U	Initial	138.6	0.164	-31.7	91.8	98.4	94.6
F10-U	1 month: 25°C/60% RH	142.8	0.173	-30.9	90.9	98.0	93.7
F10-U	3 months: 25°C/60% RH	149.5	0.189	-29.4	90.0	97.1	92.6
F10-U	6 months: 25°C/60% RH	158.2	0.211	-27.8	88.4	96.2	90.8
F10-U	1 month: 40°C/75% RH	151.1	0.202	-28.6	89.2	96.8	91.7
F10-U	3 months: 40°C/75% RH	169.3	0.251	-26.2	86.8	95.2	88.6
F10-U	6 months: 40°C/75% RH	195.4	0.318	-23.1	83.9	93.8	84.1
F10-CS1	Initial	182.4	0.203	31.2	94.6	99.1	84.2
F10-CS1	1 month: 25°C/60% RH	184.2	0.207	30.8	94.1	98.8	83.9
F10-CS1	3 months: 25°C/60% RH	187.9	0.213	30.1	93.8	98.4	83.4
F10-CS1	6 months: 25°C/60% RH	191.7	0.221	29.5	93.1	98.0	82.8
F10-CS1	1 month: 40°C/75% RH	188.6	0.216	29.7	93.4	98.2	82.9
F10-CS1	3 months: 40°C/75% RH	197.5	0.236	28.9	92.5	97.4	81.8
F10-CS1	6 months: 40°C/75% RH	210.8	0.265	27.6	91.2	96.5	80.4

Figure 17: Particle size stability trend of uncoated and coated F10 formulations over six months.

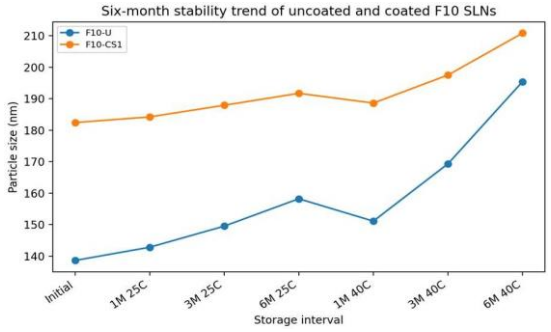

DISCUSSION

The present formulation design demonstrates how a systematic lipid-screening approach can be used to optimize a REP oral nanocarrier. The eleven uncoated formulations were intentionally structured from simple to more complex lipid matrices. Single lipids were useful for baseline comparison but did not provide the same balance of particle size and entrapment as mixed lipid systems. F10 emerged as the most promising because the combination of glyceryl monostearate, glyceryl behenate, and tristearin produced a less ordered but stable lipid matrix. This matrix likely improved drug accommodation and reduced the tendency of REP to crystallize outside the carrier. The screening results also suggest that particle size alone should not be isolated from other quality attributes. F10 showed the smallest size and excellent entrapment, but its uncoated release was rapid systems.

F10 emerged as the most promising because the combination of glyceryl monostearate, glyceryl behenate, and tristearin produced a less ordered but stable lipid matrix. This matrix likely improved drug accommodation and reduced the tendency of REP to crystallize outside the carrier.

The screening results also suggest that particle size alone should not be isolated from other quality attributes. F10 showed the smallest size and excellent entrapment, but its uncoated release was rapid. If the formulation goal were immediate dissolution enhancement only, uncoated F10 might be sufficient. However, the objective of the present work was oral bioavailability enhancement, which requires the drug to be released and absorbed in a controlled manner while avoiding premature loss. CS coating transformed F10 from a rapidly releasing nanosystem into a mucoadhesive sustained-release carrier, explaining the higher *in-vivo* exposure.

Particle size was a decisive quality attribute in the present formulation development. The uncoated SLNs showed a progressive reduction in mean particle size as the lipid matrix shifted from single-lipid systems to mixed lipid systems, with F1-F4 producing relatively larger particles (285.7-398.3 nm) and mixed formulations producing smaller and more uniform dispersions. Among the uncoated batches, F10 exhibited the smallest particle size of 138.6 nm with a PDI of 0.164, followed by F11 at 160.4 nm with a PDI of 0.188, confirming that the glyceryl monostearate, glyceryl behenate and tristearin matrix produced a compact nanodispersion. After polymer coating, particle size increased because of surface polymer deposition; F10-CS0.5 and F10-CS1 showed particle sizes of 166.8 nm and 182.4 nm, respectively, whereas F10-ALG0.5 and F10-ALG1 showed 175.3 nm and 202.5 nm. This increase was acceptable because the optimized coated formulations remained within the nanoscale range and retained suitable PDI values. The moderate size increase in F10-CS1 supported successful chitosan deposition without excessive aggregation, thereby explaining its improved mucoadhesion, controlled release and superior oral bioavailability.

The comparison between F10-CS0.5 and F10-CS1 is important. The 0.5% CS coating improved exposure compared with uncoated F10, but 1% chitosan produced the strongest outcome. This indicates that the lower coating level may not have provided a sufficiently dense mucoadhesive layer. At 1%, CS produced a stronger positive zeta potential, higher entrapment, and more sustained release. However, coating concentration cannot be increased indefinitely. Very high CS concentration could increase viscosity, particle growth, aggregation, and excessively slow release. Therefore, the 1% level appears optimal within the tested range.

ALG coating showed good stability and controlled release but lower bioavailability. This finding may be explained by the difference between retention and absorption. ALG can protect and retard release, but if the drug is not released sufficiently during the residence time in the upper intestine, systemic exposure may decrease. The anionic surface may also interact differently with mucus compared with chitosan. Although ALG coated systems may be useful for drugs requiring gastric protection or colonic release, REP may benefit more from a positively charged mucoadhesive system that promotes upper intestinal absorption. The FTIR and DSC results support the formulation mechanism. FTIR indicated that the formulation was primarily a physical incorporation system rather than a chemically modified drug.

This is favorable because chemical modification would raise safety and regulatory concerns. DSC indicated reduction of crystallinity, which explains the improved dissolution. The lipid matrix likely held REP in an amorphous or solubilized state, and the surfactant layer improved wetting. CS coating did not reverse this benefit; instead, it added surface functionality.

In-vivo enhancement may arise from multiple mechanisms. First, nanosizing increases dissolution and apparent solubility. Second, lipids stimulate bile secretion and can promote solubilization in mixed micelles. Third, lipid nanoparticles may increase lymphatic association or reduce direct exposure to hepatic first-pass metabolism, although direct lymphatic transport would require further mechanistic study. Fourth, chitosan increases intestinal residence and may transiently open tight junctions or enhance paracellular contact. Finally, sustained release keeps REP available over a longer time. The combination of these effects is consistent with the approximately 5.49-fold relative bioavailability of F10-CS1.

The pharmacodynamic glucose reduction profile should be interpreted with caution because REP effect depends on animal model, baseline glucose, feeding state, and beta-cell function. Nevertheless, the sustained reduction observed with F10-CS1 supports the pharmacokinetic data. In a final experimental manuscript, it would be important to include insulin measurements, hypoglycaemia safety observation, food intake, body weight, and histological evaluation if chronic dosing is planned. Acute pharmacodynamic data are useful, but long-term diabetes management requires repeated-dose safety and efficacy assessment.

The stability results support further development, but additional studies are required. Lipid nanoparticles can undergo polymorphic transitions from less stable to more stable crystalline forms, causing drug expulsion. The six-month observations suggest acceptable short-term robustness, but a final product should be tested for at least 12 months long-term and six months accelerated stability depending on intended dosage form. Lyophilization with cryoprotectants such as trehalose, mannitol, or sucrose may improve storage. Redispersion behavior after drying is critical because aggregation during drying can eliminate the advantage of nanosizing.

From a translational perspective, F10-CS1 offers advantages but also practical challenges. CS quality varies by molecular weight and degree of deacetylation. Its solubility depends on pH, and residual acetic acid must be controlled. The process must ensure reproducible coating thickness and surface charge. The lipid composition should be optimized for industrial procurement and batch-to-batch consistency.

The final dosage form will require additional development beyond the dispersion stage. If the product is filled as an oral nanosuspension, preservation, viscosity, dose uniformity, sedimentation, and redispersibility must be validated. If the dispersion is lyophilized, cryoprotectant screening is essential to prevent irreversible aggregation. If the lyophilized powder is filled into hard gelatin or HPMC capsules, compatibility with capsule shell moisture must be assessed. If compressed into tablets, compression pressure may damage the nanostructure unless protective matrix excipients are used. These development steps should preserve the optimized performance of F10-CS1 while creating a patient-friendly, stable, and scalable dosage form.

CONCLUSION

REP-loaded SLNs were successfully designed using hot homogenization followed by ultrasonication. Eleven uncoated formulations were screened using lipid composition as the principal variable. Among them, F10, composed of glyceryl monostearate, glyceryl behenate, and tristearin with Tween 80, showed the best nanoscale characteristics, high EE, and strong *in-vitro* release. F10 and F11 were further coated with 0.5% and 1% CS and ALG. The 1% CS coated F10 formulation (F10-CS1) produced the most favorable overall profile, including positive zeta potential, controlled release, increased AUC, and the highest relative bioavailability. HLB-based surfactant selection, high log P of REP, viscosity behavior, FTIR/SEM/TEM/DSC interpretation, coated F10 release, ng/mL pharmacokinetic reporting, relative bioavailability, and six-month stability for both coated and uncoated F10 were incorporated as corrected elements. The findings support F10-CS1 as a promising oral nanolipid platform for enhancing REP bioavailability and prolonging antihyperglycaemic activity.

REFERENCES

[1] Ebrahimi HA, Javadzadeh Y, Hamidi M, Jalali MB. REP-loaded solid lipid nanoparticles: effect of using different surfactants/stabilizers on physicochemical properties of nanoparticles. Daru. 2015;23:46.

[2] Rawat MK, Jain A, Singh S. In vivo and cytotoxicity evaluation of REP-loaded binary lipid matrix based solid lipid nanoparticles. J Pharm Sci. 2011;100(6):2366-2378.

[3] Milner Z, Jha S. REP. In: StatPearls. Treasure Island (FL): StatPearls Publishing; 2023.

[4] Amidon GL, Lennernas H, Shah VP, Crison JR. A theoretical basis for a biopharmaceutic drug classification: correlation of in vitro drug product dissolution and in vivo bioavailability. Pharm Res. 1995;12(3):413-420.

[5] Ahmad M, Alkahtani S, Ahmad J, et al. Formulation and optimization of REP nanoparticles using microfluidics for enhanced bioavailability and management of diabetes. Biomedicines. 2023;11(4):1064.

[6] US Food and Drug Administration. PRANDIN (REP) tablets: prescribing information. Silver Spring: FDA; 2019.

[7] European Medicines Agency. REP product information. Amsterdam: EMA; 2024.

[8] Muller RH, Mader K, Gohla S. Solid lipid nanoparticles for controlled drug delivery: a review of the state of the art. Eur J Pharm Biopharm. 2000;50(1):161-177.

[9] Mehnert W, Mader K. Solid lipid nanoparticles: production, characterization and applications. Adv Drug Deliv Rev. 2001;47(2-3):165-196.

[10] Mishra V, Bansal KK, Verma A, Yadav N, Thakur S, Sudhakar K, et al. Solid lipid nanoparticles: emerging colloidal nano drug delivery systems. Pharmaceutics. 2018;10(4):191.

[11] Ganesan P, Ramalingam P, Karthivashan G, Ko YT, Choi DK. Recent developments in solid lipid nanoparticle and surface-modified solid lipid nanoparticle delivery systems for oral delivery. Int J Nanomedicine. 2018;13:1569-1583.

[12] Shah R, Eldridge D, Palombo E, Harding I. Lipid nanoparticles: production, characterization and stability. Cham: Springer; 2015.

[13] Jannin V, Blas L, Chevrier S, Miolane C, Demarne F, Spitzer D. Evaluation of the digestibility of solid lipid nanoparticles of glyceryl dibehenate. Eur J Pharm Sci. 2018;111:91-95.

[14] Doktorovova S, Souto EB, Silva AM. Hansen solubility parameters for prescreening formulation of solid lipid nanoparticles. Pharm Dev Technol. 2018;23(1):96-105.

[15] Qushawy M, Nasr A. Solid lipid nanoparticles as nano drug delivery carriers: preparation, characterization and application. Int J App Pharm. 2020;12:1-9.

[16] Luo Y, Teng Z, Li Y, Wang Q. Solid lipid nanoparticles for oral drug delivery: chitosan coating improves stability, controlled delivery, mucoadhesion and cellular uptake. Carbohydr Polym. 2015;122:221-229.

[17] Agnihotri SA, Mallikarjuna NN, Aminabhavi TM. Recent advances on chitosan-based micro- and nanoparticles in drug delivery. J Control Release. 2004;100(1):5-28.

[18] George M, Abraham TE. Polyionic hydrocolloids for the intestinal delivery of protein drugs: alginate and chitosan. J Control Release. 2006;114(1):1-14.

[19] Pandey SS, Patel MA, Bhatt N, et al. Bioavailability enhancement of REP from nanostructured lipid carrier based delivery system. J Drug Deliv Sci Technol. 2020;59:101903.

[20] Karami Z, Saghatchi Zanjani MR, Hamidi M. Improved oral bioavailability of REP, a typical BCS class II drug, with lipid based nanoformulations. J Biomed Mater Res B Appl Biomater. 2020;108(8):3187-3198.

[21] Ali HSM, Aboud HM, Elkomy MH, et al. REP solid lipid nanoparticles in chitosan patches for controlled release and improved therapeutic performance. Int J Nanomedicine. 2024;19:1-18.

[22] Fatouh AM, Elshafeey AH, Abdelbary A. Intranasal agomelatine solid lipid nanoparticles to enhance brain delivery: formulation, optimization and in vivo pharmacokinetics. Drug Des Devel Ther. 2017;11:1815-1831.

[23] Yang XD, Zhang Y, Wang X, et al. Dissolution rate enhancement of REP by solid dispersion technique. Asian J Pharm Sci. 2016;11:459-466.

[24] Costa P, Lobo JMS. Modeling and comparison of dissolution profiles. Eur J Pharm Sci. 2001;13(2):123-133.

[25] Higuchi T. Mechanism of sustained-action medication: theoretical analysis of rate of release of solid drugs dispersed in solid matrices. J Pharm Sci. 1963;52(12):1145-1149.

[26] Korsmeyer RW, Gurny R, Doelker E, Buri P, Peppas NA. Mechanisms of solute release from porous hydrophilic polymers. Int J Pharm. 1983;15(1):25-35.

[27] International Council for Harmonisation. ICH Q1A(R2): Stability testing of new drug substances and products. Geneva: ICH; 2003.

[28] Souto EB, Muller RH. Lipid nanoparticles: effect on bioavailability and pharmacokinetic changes. Handb Exp Pharmacol. 2010;197:115-141.

[29] [29] Doktorovova S, Souto EB. Nanostructured lipid carrier-based hydrogel formulations for drug delivery: a comprehensive review. Expert Opin Drug Deliv. 2009;6(2):165-176.

[30] [30] Patel VR, Agrawal YK. Nanosuspension: an approach to enhance solubility of drugs. J Adv Pharm Technol Res. 2011;2(2):81-87.

[31] [31] Shaik ZB, Pathan AA, Lingabathula H. Formulation of uncoated and polymer-coated solid lipid nanoparticles to enhance oral bioavailability of pitavastatin calcium. Journal of Applied Bioanalysis. 2025;11(11s):612-62